© 2014. Published by The Company of Biologists Ltd | Journal of Cell Science (2014) 127, 1537–1549 doi:10.1242/jcs.140780

RESEARCH ARTICLE

Fast axonal transport of the proteasome complex depends on membrane interaction and molecular motor function

Maria G. Otero[1], Matías Alloatti[1], Lucas E. Cromberg[1], Angels Almenar-Queralt[2], Sandra E. Encalada[2,*], Victorio M. Pozo Devoto[1], Luciana Bruno[3], Lawrence S. B. Goldstein[2] and Tomás L. Falzone[1,‡]

ABSTRACT

Protein degradation by the ubiquitin-proteasome system in neurons depends on the correct delivery of the proteasome complex. In neurodegenerative diseases, aggregation and accumulation of proteins in axons link transport defects with degradation impairments; however, the transport properties of proteasomes remain unknown. Here, using *in vivo* experiments, we reveal the fast anterograde transport of assembled and functional 26S proteasome complexes. A high-resolution tracking system to follow fluorescent proteasomes revealed three types of motion: actively driven proteasome axonal transport, diffusive behavior in a viscoelastic axonema and proteasome-confined motion. We show that active proteasome transport depends on motor function because knockdown of the KIF5B motor subunit resulted in impairment of the anterograde proteasome flux and the density of segmental velocities. Finally, we reveal that neuronal proteasomes interact with intracellular membranes and identify the coordinated transport of fluorescent proteasomes with synaptic precursor vesicles, Golgi-derived vesicles, lysosomes and mitochondria. Taken together, our results reveal fast axonal transport as a new mechanism of proteasome delivery that depends on membrane cargo 'hitch-hiking' and the function of molecular motors. We further hypothesize that defects in proteasome transport could promote abnormal protein clearance in neurodegenerative diseases.

KEY WORDS: Axonal transport, Membrane interaction, Molecular motors, Proteasome, Vesicles, Kinesin-1

INTRODUCTION

Local protein homeostasis in highly polarized neurons is supported by a regulated system of protein delivery by axonal transport and a coordinated action of protein removal by selective degradation (Bingol and Sheng, 2011; Stokin and Goldstein, 2006). The localization of the ubiquitin-proteasome system (UPS) has emerged as an important regulator of synaptic function, and local proteasome degradation defects have been implicated during the progression of many neurodegenerative diseases (Oddo, 2008; Yi and Ehlers, 2007). However, little is known about the intracellular mechanisms of the distribution of the proteasome and their axonal transport properties that assure the proper delivery and positioning of the proteasome complex in neurons.

Protein turnover by the UPS involves the identification of targets and their tagging with a polyubiquitin chain as the signal for specific degradation by the proteasome complex (Ciechanover and Brundin, 2003). The 26S proteasome barrel is assembled through the interaction of the 20S catalytic core, which comprises four rings of α and β subunits, with the 19S regulatory particle (Murata et al., 2009). Several synaptic proteins have been shown to undergo local UPS-mediated turnover, suggesting a compartment-specific function for the 26S complex (Ehlers, 2003; Patrick, 2006). In response to neuron depolarization, proteasomes can be rapidly recruited to dendritic spines by a mechanism that is not fully understood (Bingol and Schuman, 2006; Bingol et al., 2010), leading to a confined turnover of polyubiquitinated proteins (Djakovic et al., 2009; Ehlers, 2003) that supports a compartmentalized function of the proteasome at synapses (Upadhya et al., 2006; Zhao et al., 2003). Proteasome-mediated degradation is involved in the clearance of abnormal protein aggregates and proteasome defects have been associated with a number of neurodegenerative diseases (Ciechanover and Brundin, 2003). Local dysfunction of proteasome-dependent degradation is associated with the early phases of synaptic defects in tauopathies, including the formation of inclusion bodies that contain the ubiquitinated form of the microtubule-associated protein tau (Tai et al., 2012).

Axonal transport, carried out by molecular motors, supports neuronal function by the correct delivery and positioning of proteins and organelles (Stokin and Goldstein, 2006). Kinesin motors drive the anterograde axonal transport towards the synapses by walking the microtubules to the plus end, whereas dynein complexes support the retrograde transport to cell bodies by walking to the minus end of microtubules (Hirokawa et al., 2010). Fast axonal transport is mediated by membrane-associated cargos that have been described as interacting specifically with kinesin and dynein motors (Goldstein, 2003; Karki and Holzbaur, 1999). Cytosolic proteins undergo slow axonal transport, which has also been shown to depend on an interaction with molecular motors that is mediated by adaptor proteins (Terada et al., 2010). This slow average speed of soluble proteins depends on a probabilistic association with carriers that move under fast transport (Lasek et al., 1984; Scott et al., 2011). In support of this view, recent data has shown an axonal diffusion, with an anterograde bias, of synapsin that was mediated by the flux of fast moving vesicles (Tang et al., 2013). However, little is known

[1]Instituto de Biología Celular y Neurociencias (UBA-CONICET), Facultad de Medicina, Universidad de Buenos Aires, Buenos Aires CP 1121, Argentina. [2]Department of Cellular and Molecular Medicine, School of Medicine, University of California San Diego, La Jolla, CA 92093, USA. [3]Departamento de Física y IFIBA-CONICET, Facultad de Ciencias Exactas y Naturales, Universidad de Buenos Aires, Buenos Aires CP 1428, Argentina.
*Present address: Department of Molecular and Experimental Medicine, Dorris Neuroscience Center, The Scripps Research Institute La Jolla, CA 92037, USA.

‡Author for correspondence (tfalzone@fmed.uba.ar)

Received 16 August 2013; Accepted 22 January 2014

Journal of Cell Science (2014) 127, 1537–1549 doi:10.1242/jcs.140780

about the transport modes that mediate the movement of large cytoplasmic protein complexes, such as the proteasome, along axons. Studies of fluorescently labeled proteasomes have suggested that, in human fibrosarcoma cells, the distribution of proteasomes occurs through cytoplasmic diffusion at a steady state (Reits et al., 1997), whereas *in vivo* and *in vitro* analyses have suggested that proteasomes associate with lipid membranes (Kalies et al., 2005; Newman et al., 1996), and that this interaction could support a mechanism for the long-range movement of proteasomes in neurons.

Disruption of the microtubule-based transport system results in organelle accumulation and axonal swellings, which can be further increased by impairments in the protein clearance pathways (Stokin and Goldstein, 2006). In neurodegenerative diseases, impaired protein degradation has been suggested to occur through specific proteasome inhibition that is exerted by abnormal aggregated proteins (Tai et al., 2012; Tseng et al., 2008) and by the proteasome defects that have been described in different areas of the brains of patients with Alzheimer's disease (Keck et al., 2003; Keller et al., 2000). Interestingly, failures in the UPS lead to the accumulation of aggregated proteins in axons (Tai and Schuman, 2008), and protein accumulation is, in turn, associated with defects in axonal transport (Stokin and Goldstein, 2006). Thus, the confined accumulation of polyubiquitinated aggregates that is observed during neurodegeneration raises the possibility that impairments in the distal axonal delivery of UPS components play central roles in disease progression (Bence et al., 2001; Oddo, 2008; Rubinsztein, 2006). Similar abnormal function of the proteasome can be predicted during impairment of axonal transport because kinesin-1 defects enhance protein accumulation, axonopathies and neurodegeneration in mouse models of Alzheimer's disease (Falzone et al., 2009; Stokin et al., 2005). Recently, a link between proteasomes and motors in mammalian cells has been suggested to occur through the proteasome-associated protein ECM29, which is involved in proteasome assembly (Gorbea et al., 2010). This interaction indicates a molecular mechanism for motor-protein-dependent transport of the proteasome complex.

Here, using *in vivo* and live-cell imaging experiments, we test the novel hypothesis that the proteasome complex is actively transported along axons. By using short-term mouse sciatic nerve ligations, we also show fast anterograde transport of the functional 26S proteasome complex. We developed a high-resolution time and space live-imaging setup to track and describe the movement of fluorescent α4 core proteasome subunits in axons, allowing characterization of three new and independent modes of proteasome motion – (1) actively driven transport, (2) diffusion in a viscoelastic axonema and (3) trapped proteasomes with confined motion. We demonstrate that knockdown of the KIF5B motor protein results in a reduction of the anterograde proteasome flux on axons and a decrease in the density of anterograde segmental velocities, which suggests that proteasome transport partially depends on kinesin-1 cargos for their delivery to distant sites. Finally, we show that fast and processive axonal transport of proteasomes depends on the association of proteasomes with intracellular membranes, and describe the coordinated movement of proteasomes with different vesicles and membrane organelles. Taken together, our results describe three previously unknown modes of proteasome movement in axons and, furthermore, uncover a novel mechanism of fast axonal transport of this large and active complex that is dependent upon membrane cargo 'hitch-hiking' and the function of molecular motors. Therefore, we suggest that distant neuronal protein degradation depends on a mechanism of proteasome delivery that, when impaired, can have profound implications for the clearance of local proteins, similar to that observed during the progression of neurodegenerative diseases.

RESULTS

In vivo fast axonal transport of active proteasomes in mouse sciatic nerves

Local UPS-mediated degradation suggests that there are active proteasomes at synapses (Bingol and Sheng, 2011; Yi and Ehlers, 2007), but how proteasome components arrive at neuronal termini is unknown. To test whether neuronal proteasomes are transported along axons *in vivo*, we performed staining of short-term mouse sciatic nerve ligations to analyze representative components of the complex. The accumulation of proteins at the proximal or distal side of an obstructed nerve is indicative of their anterograde or retrograde axonal transport, respectively (Fig. 1A). After ligation, core (α and β) and regulatory (Mss1, also known as PSMS2) subunits of the proteasome showed significant accumulation at the proximal side of the ligation compared with that in distal or unligated nerves (Fig. 1B,C). Quantification of the accumulated integrated fluorescent intensity, normalized to phosphorylated neurofilament staining, revealed a twofold increase of proteasome subunits in proximal ligated nerves compared with that in distal ligated nerves (Fig. 1B,C). As a control for proximal accumulation, nerves were stained for the transmembrane amyloid precursor protein (APP), which moves in a net anterograde direction (supplementary material Fig. S1). To determine further whether proteasomes accumulate at the proximal side within axons, and not through induced expression in glia, we examined nerve cross-sections in ligated and unligated nerves. In unligated nerves, the core β5 subunit of the proteasome was found in axons and Schwan cells, as shown by co-staining for phosphorylated neurofilament (an axonal marker) and the glial marker S100; however, after ligation, a substantial accumulation of β5 was observed within axons (Fig. 1D). Similar results were obtained for the regulatory proteasome subunit Mss1 (Fig. 1E). To exclude artifacts that can arise from glia-induced expression after nerve trauma, two ligations were generated along the sciatic nerve. Double-ligation experiments showed the proximal accumulation of proteasome subunits only at the node closest to the cell body, whereas proteasomes did not accumulate proximally to the second node (Fig. 1H). This result confirms that axonal transport mediates the increase of proteasome subunits and not the ligature itself.

To gain insight about the functionality of accumulated proteasome subunits in axons, we tested for the presence of protein polyubiquitination as a canonical signal for degradation after ligation (Bossy-Wetzel et al., 2004). Analysis by western blotting of ligated nerve homogenates showed a large accumulation of polyubiquitinated proteins at both proximal and distal ligated nerves when compared with those from unligated nerves (Fig. 1F). To determine whether the observed proximal accumulation of proteasome subunits is associated with an increase in protein degradation, we measured proteasome activity from nerve homogenates using a fluorescence assay. Quantification of the fluorescence released after proteasome-dependent peptide hydrolysis revealed a significant increase in activity in the proximal region compared with unligated nerve homogenates (Fig. 1G). Taken together, these results suggest that proteasomes

Journal of Cell Science (2014) 127, 1537–1549 doi:10.1242/jcs.140780

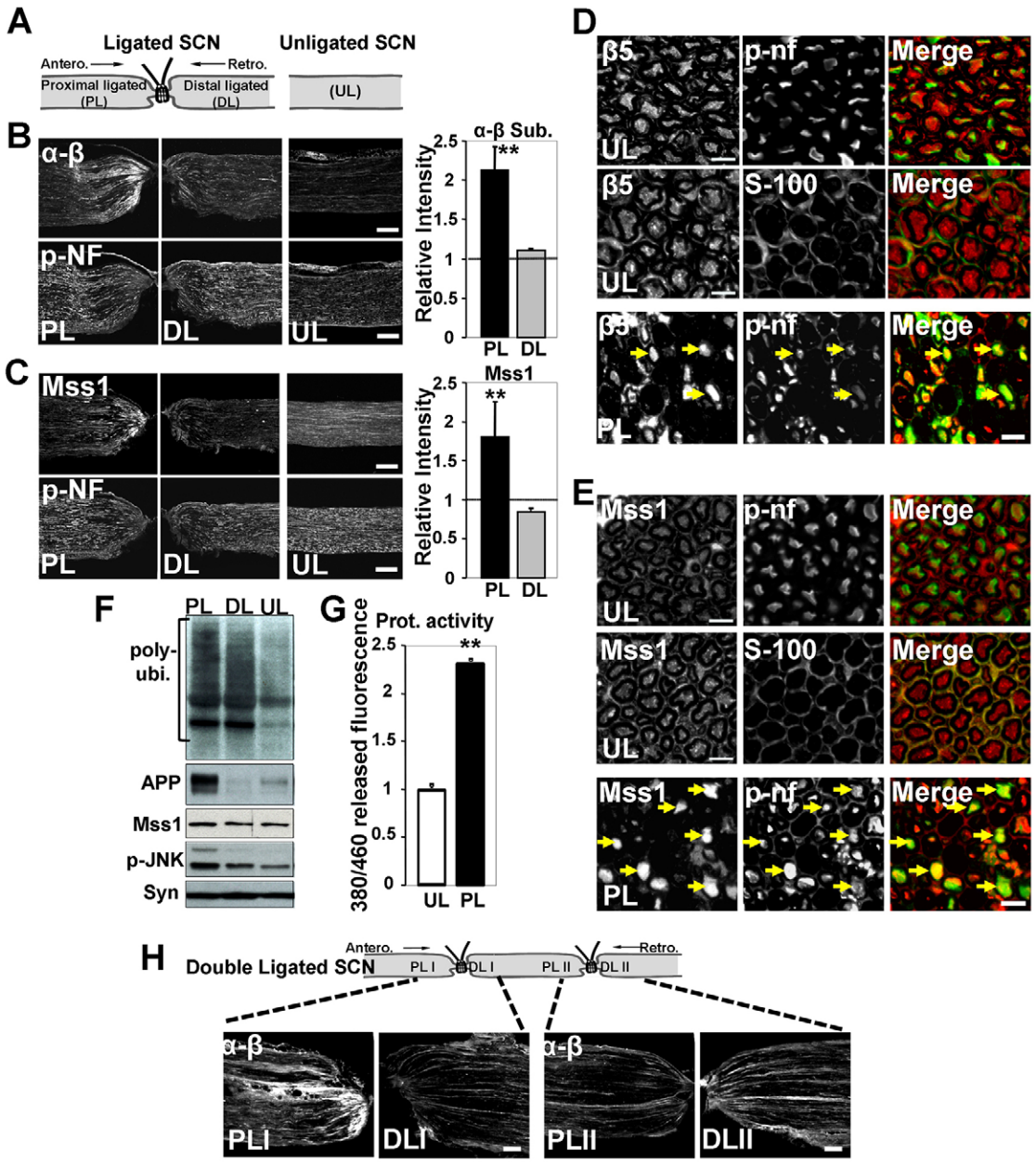

Fig. 1. *In vivo* fast axonal transport of active proteasomes. (A) Proximal (PL), distal (DL) and unligated (UL) sides of the sciatic nerve used in staining and western blots. (B,C) Confocal images of proximal ligated, distal ligated or unligated mouse sciatic nerves showing α-β or Mss1 proteasome subunits and phosphorylated neurofilaments (p-NF). Scale bars: 50 μm. Quantification of α-β and Mss1 integrated fluorescent intensity from PL and DL nerves, normalized to p-NF and taking UL as 1. $^{**}P<0.02$, Student's *t*-test, $n=4$ experiments. (D,E) Cross-sections of UL and PL nerves showing β5 (D) and Mss1 (E) staining in axons (p-nf) and Schwann cells (S-100). Arrows indicate accumulation of the β5 subunit and Mss1 at the PL in axons. Scale bars: 10 μm. (F) Western blotting of homogenates from PL, DL and UL nerves showing polyubiquitylated proteins. Synuclein (Syn) was used as a loading control. APP and p-JNK were used as proximal accumulation controls. (G) Proteasome activity in UL and PL nerve homogenates (40 μg) measured by the release of fluorescence (λ380–460) after peptide hydrolysis using a proteasome probe. $^{**}P<0.02$, Student's *t*-test, $n=3$. (H) Images taken, by using a confocal microscope, of double-node experiments on mouse sciatic nerves showing the staining of α-β proteasome subunits at locations proximal and distal from the first (I) and second (II) ligation nodes. Note the accumulation of proteasome subunits only at the PLI side of the nerve.

undergo fast axonal transport, and that this movement mediates the accumulation of functional complexes that are involved in the degradation of local polyubiquitinated proteins.

Fast and processive proteasome axonal transport in cultured hippocampal neurons

Cargos transported along axons display unique distributions and localizations that depend upon the motor molecules and their dynamic properties. In agreement with previous studies (Mengual et al., 1996), cultured murine hippocampal neurons showed a diffuse distribution of the core proteasome subunits in cell bodies (Fig. 2A), dendrites (Fig. 2B), axons (Fig. 2C) and growth cones (Fig. 2D). To analyze their distribution and the axonal transport properties of proteasomes in central neurons, we generated a vector driving the expression of the mouse proteasome α4 core subunit (PSMA4) fused to the yellow fluorescent protein (YFP)

Journal of Cell Science (2014) 127, 1537–1549 doi:10.1242/jcs.140780

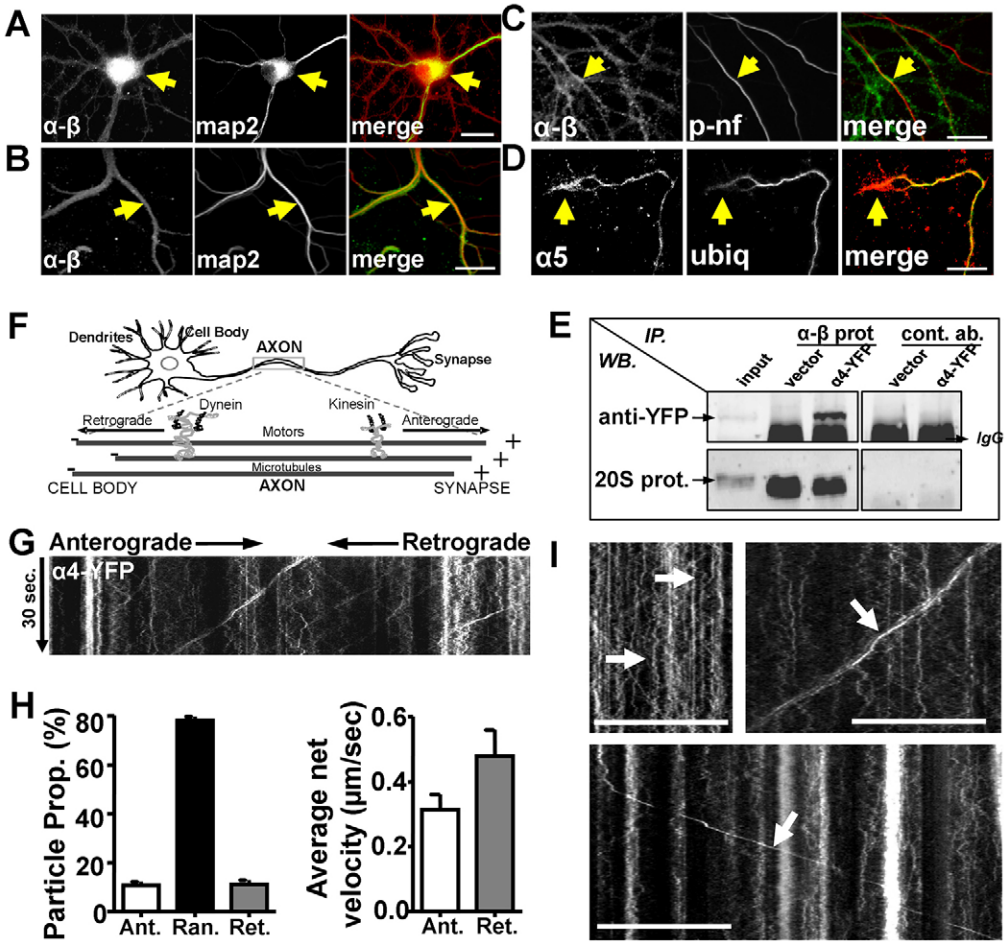

Fig. 2. Axonal transport of α4–YFP proteasome subunits in axons. (A–D) Images of 10-day-old mature hippocampal neurons that show the distribution of α-β proteasome subunits (yellow arrows) in cell bodies (A, map2), dendrites (B, map2), axons (C, p-nf) and growth cones (D, α5 subunit plus ubiquitin). (E) Immunoprecipitation (IP) of the proteasome by using pan-antibody against α-β subunits from control (vector) or N2a cells that had been transfected with CMV-α4-YFP. Control IPs were performed using nonspecific antibodies. IP eluates were probed using antibodies against YFP (α4–YFP) or the 20S proteasome. (F) The setup used to record movies of anterograde and retrograde axonal transport in hippocampal neurons. To the right and left are plus- and minus-oriented microtubules, respectively (see supplementary material Fig. S2). (G) Kymograph of time against distance obtained from a 30-second movie generated at 8 frames/second in an axon transfected with α4–YFP (supplementary material Movie 1). Scale bar: 20 μm. (H) Average proportion of α4–YFP particles moving in an anterograde (ant), retrograde (ret) or random (ran) direction (left panel) and average net velocities for moving α4–YFP particles (right panel). $n=30$ neurons, 638 particles. (I) Kymographs showing the heterogeneous behavior of moving α4–YFP puncta and examples of clear processive anterograde or retrograde particles (arrows). Scale bars: 20 μm (A,G,I); 10 μm (B–D).

under the control of the cytomegalovirus promoter (CMV-α4-YFP). The incorporation of fluorescently tagged α4 subunits into assembled proteasome complexes was shown by co-immunoprecipitation of α4–YFP with endogenous proteasomes in transfected neuroblastoma (N2a) cells (Fig. 2E). To measure axonal transport, we identified and selected axonal projections by analyzing the localization of fluorescently tagged marker proteins that had been transfected into the cells (Fig. 2F; supplementary material Fig. S2A); polarized microtubule orientation in axons was confirmed by expression of the microtubule cap protein EB3 (also known as Mapre3) tagged with red fluorescent protein (EB3–RFP; supplementary material Fig. S2B,C). Continuous live-imaging recordings at 125 mseconds (8 frames/second) in hippocampal neurons that had been transfected with CMV-α4-YFP allowed the generation of kymographs that revealed a large amount of heterogeneous proteasome motion (Fig. 2G; supplementary material Movie 1). Analysis of the kymographs showed α4–YFP particles that had trajectories that resembled random motion behavior with no overall movement; however, we also observed clear processive trajectories that corresponded to anterograde and retrograde axonal transport of α4–YFP (Fig. 2H,I). Quantification of the α4–YFP processive puncta revealed fast anterograde and retrograde average net velocities that correlate with molecular motor-dependent axonal transport (Fig. 2H,I).

High spatial- and temporal-resolution analyses identify three different types of proteasome motion

To analyze further the heterogeneous motion of proteasomes in the axon and to relate it to different distribution mechanisms, we developed a high-resolution space- and temporal-tracking system. We obtained highly detailed kymographs by increasing the temporal resolution of the live-imaging recording to 20 mseconds (50 frames/second) in hippocampal neurons that had been transfected with CMV-α4-YFP (Fig. 3A; supplementary material Movie 2). Single particles were tracked using an

Journal of Cell Science (2014) 127, 1537–1549 doi:10.1242/jcs.140780

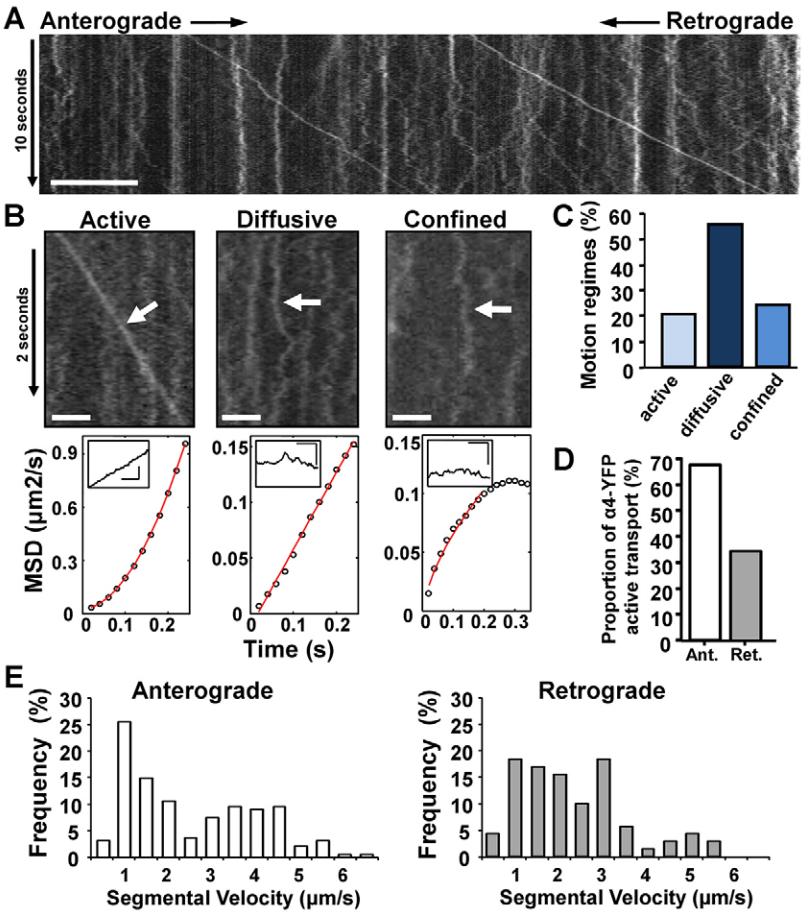

Fig. 3. High-resolution analysis of proteasome trajectories revealed three patterns of proteasome movement in axons. (A) Kymograph obtained from a continuous movie (supplementary material Movie 2) recording at 20 mseconds/frame (50 frames/second) showing detailed trajectories of α4–YFP particles. Scale bar: 10 μm. (B) Upper panel: image crops showing high-magnification kymographs (100 data point sets) corresponding to proteasome particles undergoing active transport, random diffusion and confined motion, respectively. (Arrows indicate particle tracks.) Scale bars: 2 μm. Lower panel: recovered trajectories from kymographs shown in the upper panel with their corresponding mean square displacement (MSD). MSD data was fitted to an anomalous model $MSD\tau^{\alpha}$. The corresponding fittings are shown in red (α=2, 1 and 0.4). Insets within each graph show the recovered trajectories as a function of space versus time. Horizontal and vertical scale bars in insets represent 0.5 seconds and 2 μm, respectively. (C) Proportion of active transport, diffusive movement and confined motion obtained from 670 particle segments (100 data set points) generated using 317 single proteasome tracked particles from 87 imaged neurons. Results taken from five transfection experiments. (D) The proportion of anterograde versus retrograde segmental velocities. n=259. (E) The distribution of segmental velocities (%) obtained from proteasome particles undergoing anterograde and retrograde active axonal transport.

algorithm developed to identify the position with a sub-pixel resolution, and recovered trajectories were then cut into segments of 100 data points (see Materials and Methods). The mean square displacement (MSD) was computed for each segment using Eqn 1 and fitted to the empirical expression given by Eqn 2, as described in Materials and Methods (Fig. 3B). Proteasome trajectories were then classified as actively driven, diffusive or confined according to the dependence of the MSD with time (Fig. 3B). By using 500 MSDs obtained from more than 300 trajectories, we identified 20% of proteasome particles as having an actively driven trajectory, 56% of particles exhibited a diffusive-like motion and the remaining 24% of particles displayed a confined proteasome motion (Fig. 3C).

To investigate further these three different types of proteasome motion, we first determined the distributions of the segmental velocities obtained for the actively driven anterograde and retrograde proteasome trajectories. Each processive trajectory was further divided into segments, and the mean velocity of the segment was computed from the slope of the position against time plot. We obtained a higher proportion of anterograde recovered segmental velocities compared with retrograde ones (Fig. 3D). A range of segmental velocities for anterograde and retrograde proteasomes (Fig. 3E) were measured that are comparable to the velocities reported for vesicles undergoing kinesin- and dynein-mediated fast axonal transport (Reis et al., 2012). Diffusive-like trajectories, characterized by a linear dependence of the MSD with the time lag, allowed the calculation of a diffusion coefficient of 0.0584±0.0056 μm^2/second (mean±s.e.m.; Materials and Methods) that is consistent with the molecular size of a proteasome complex that diffuses in a viscous axonema (Bohn et al., 2010; Popov and Poo, 1992). By contrast, confined proteasome trajectories showed a plateau in the MSD plot (Fig. 3B), which determines a confinement region of 0.72± 0.03 μm in size (Materials and Methods). The density distribution function obtained from confined single-particle trajectories showed that the constraint exerted over the proteasome is less than that exerted by elastic binding trapping (Jin et al., 2007), suggesting that the movement of a confined proteasome is bound by a 'cage' (supplementary material Fig. S3A). Taken together, these results reveal that there are three different modes of proteasome motion and, more importantly, describe the processive movement of particles that display distributions with high segmental velocities that result from the fast axonal transport of proteasomes.

Knockdown of the kinesin-1 motor impairs fast axonal transport of the proteasome

To test whether actively driven proteasomes depend on molecular motor function, we knocked down *kif5b*, one of the three kinesin-1 heavy chain subunits that has been shown previously to alter certain cargos (Encalada et al., 2011), and analyzed proteasome movement. Efficient knockdown of KIF5B was shown by western blotting lysates from N2a cells transfected with an shRNA against *kif5b* (shKif5b), when compared with control (Fig. 4A,B), and by immunofluorescent staining of hippocampal neurons (Fig. 4C,D). To study processive trajectories for a longer period of time, we acquired movies at 8 frames/second. This rate allowed the

Journal of Cell Science (2014) 127, 1537–1549 doi:10.1242/jcs.140780

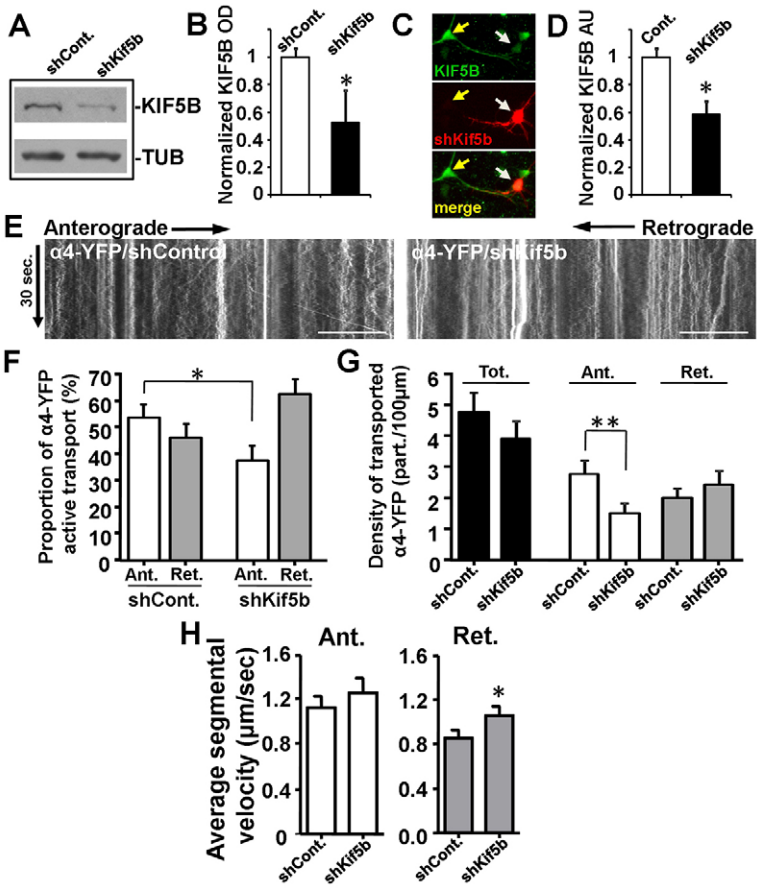

Fig. 4. Reduction of the KIF5B motor protein impairs proteasome axonal transport. (A) Western blotting of the KIF5B protein from N2a cells transfected with a control shRNA (shControl) or shRNA against *kif5b* (shKif5b) for 48 hours. Tubulin was used as a loading control. (B) Integrated optical density (OD) quantification for normalized KIF5B protein levels in shControl- and shKif5b-transfected cells from four independent experiments. *$P<0.05$, Student's *t*-test. (C) Staining with an antibody against KIF5B shows the level of protein in untransfected (control) hippocampal neuron (yellow arrow) compared with cells transfected with shKif5b (white arrow). (D) Integrated intensity (AU, arbitrary units) quantification in control neurons compared with those transfected with shKif5b. $n=10$ neurons. *$P<0.05$, Student's *t*-test. (E) Kymographs generated from 30-second movies (supplementary material Movies 3, 4) showing α4–YFP movement in control (α4–YFP/shControl) and shKif5b-transfected cells (α4–YFP/shKif5b). Scale bars: 20 μm. (F) The proportion of anterograde versus retrograde segmental velocities. *$P<0.05$, Mann–Whitney test, $n=268$ particles in control cells, 141 particles in shKif5b-transfected cells. (G) The mean total (Tot.), anterograde (Ant.) and retrograde (Ret.) density of actively transported proteasomes expressed as segments in 100 μm of axonal length. **$P<0.02$, Mann–Whitney test. (H) Anterograde and retrograde mean segmental velocities for α4–YFP and shControl, and α4–YFP and shKif5b cells. $n=5$ experiments. Kymographs analyzed $n=51$ segments from control cells, 45 segments for shKif5b-transfected cells. *$P<0.05$.

recovery of long-range transport of the proteasome from neurons that had been co-transfected with α4–YFP and shKif5b or a control shRNA (Fig. 4E; supplementary material Movies 3, 4). Moving proteasome particles were tracked by using the algorithm, and the MSDs were calculated for the trajectories of particles in control or shKif5b-transfected cells to discard segments without active transport. Hippocampal neurons with reduced levels of KIF5B exhibited a significant reduction in the proportion of proteasomes that had anterograde segmental velocities, consequently the proportion of proteasomes that showed retrograde velocities increased compared with control (Fig. 4F). Interestingly, this change in the segmental velocity flux was observed because of a selective and significant reduction in the density of anterograde proteasome segments, whereas the average retrograde number was not significantly impaired (Fig. 4G). We observed a clear change in the anterograde flux, but the average segmental velocity of anterograde proteasomes was similar between control and shKif5b-transfected cells; by contrast, a small increase in the average retrograde segmental velocities was observed in cells transfected with shKif5b (Fig. 4H). To test for an interaction between axonal proteasomes and moving kinesin-1 cargos, hippocampal neurons that had been transfected with α4–YFP were stained with an antibody against KIF5B. Imaging of mature axonal projections, by using confocal microscopy, showed a few proteasome particles that consistently colocalized with KIF5B staining (supplementary material Fig. S3B). Taken together, these results reveal kinesin-1, and in particular KIF5B, as one of the microtubule-associated molecular motors that contribute to the fast anterograde axonal transport of the proteasome complex.

Neuronal proteasomes associate with membranes and fractionate with synaptosome vesicles

Little is known about how the proteasome is shuttled within neurons; however, we observed proteasome particles moving with fast and processive velocities that were partially dependent upon the function of kinesin-1, which is reminiscent of intracellular-membrane-associated movement. To determine whether proteasomes are associated with membranes *in vivo*, we fractionated mouse brain homogenates by using bottom-loaded continuous sucrose gradients to identify proteins associated with membranes. Bona fide soluble proteins (ubiquitin) remained at the bottom of the gradient, whereas transmembrane proteins [APP, synaptotagmins and syntaxin 13 (STX12) fractionated at different densities (Fig. 5A). The soluble and membrane-bound dynein heavy chain (DYNC1H1) motor showed a wide distribution along fractions (Fig. 5A). As expected, a proportion of core α5 (PSMA5), β5 (PSMB5) and regulatory Mss1 proteasome subunits remained in soluble fractions, whereas a substantial percentage (ranging from 20% to 30%) separated within fractions 5 to 13, which are enriched in membrane-associated proteins (Fig. 5B). The similar fractionation pattern displayed for the different subunits suggests that proteasomes are tightly assembled and associated with membranous organelles.

As similar patterns of fractionation were displayed by proteasome subunits and the synaptic marker synaptotagmin, we tested whether proteasomes associate with synaptic membranes. Synaptosomes that had been purified from adult mouse brains showed the presence of α5 and β5 core proteasome subunits from the 20S complex in the synaptosome-enriched fraction (LP2)

Journal of Cell Science (2014) 127, 1537–1549 doi:10.1242/jcs.140780

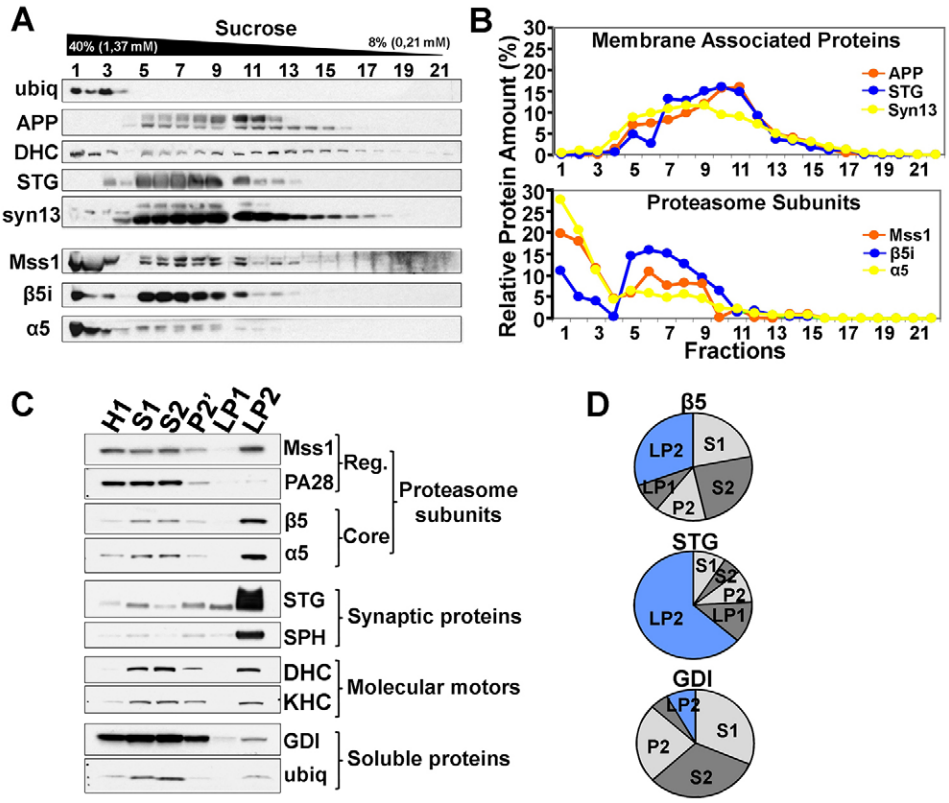

Fig. 5. Neuronal proteasomes associate with membrane and fractionate with synaptic vesicles. (A) Bottom-loaded sucrose density fractions of brain homogenates. The separation of the proteasome α5, β5 and Mss1 subunits compared with soluble ubiquitin and membrane-associated proteins [APP, synaptotagmin (STG) and syn13]. (B) The relative protein distribution plotted from the sucrose density fractionation experiments normalized to the total protein. Note the proteasomes in the soluble (1–3) and low-density (5–13) fractions. (C) Synaptosome purification from mouse brain cortices loaded as homogenate (H1), soluble (S1, S2), plasma membrane (LP1) and synaptosome-enriched (LP2) fractions. α5, β5, Mss1 and PA28 subunits of the proteasome. Synaptic proteins, STG and SPH; molecular motors, KHC and DHC; and soluble proteins, GDI and ubiquitin. (D) The proportion of β5, STG and GDI protein enriched in the LP2 fraction (blue) compared to other fractions.

(Fig. 5C,D). As expected, we also observed enrichment in this fraction of synaptic transmembrane proteins – synaptotagmin and synaptophysin (SPH, also known as SYP) – as well as kinesin and dynein motors (Abe et al., 2009) (Fig. 5C,D). The cytosolic protein GDP dissociation inhibitor (GDI, also known as GDI1) and free ubiquitin remained soluble and detected at very low levels in LP2 (Fig. 5C,D). Interestingly, the Mss1 subunit from the 19S regulatory particle was present in LP2, whereas the PA28α (PSME1) subunit from the ubiquitin-independent proteasome was not (Fig. 5C), suggesting that the 26S complex, which is associated with polyubiquitin-dependent degradation, is localized to synaptosomal domains. Taken together, these results indicate that proteasomes associate with membranes that can mediate their distribution throughout the neuron.

Proteasome processive particles 'hitch-hike' on multiple membranous organelles for their coordinated fast axonal transport

To test whether the profile of moving proteasomes depends on the interaction with one or many subcellular organelles, we acquired sequential movies that simultaneously monitored fluorescently tagged α4 proteasome subunits and fluorescent vesicle markers in neurons. Owing to the presence of proteasome subunits in synaptosomes, and to test whether proteasomes are co-transported with synaptic components, we co-transfected cells with vectors encoding the α4 subunit tagged with mCherry (α4–Cherry) and synaptophysin fused to GFP (SPH–GFP) (Fig. 6A; supplementary material Movie 5). Movement of both tagged proteins was monitored by recording double-color movies, recording sequentially in the red (α4–Cherry) and then green (SPH–GFP) channel (back and forth, 15 seconds in each channel). Clearly observable processive trajectories that were common to both proteasomes and synaptophysin were identified and quantified, revealing an association between processive proteasomes and SPH-containing vesicles (Fig. 6B,I). Because a small percentage of moving proteasomes were associated with synaptophysin, we tested whether proteasomes could also associate with other Golgi-derived membranes, such as the APP vesicle (Fig. 6C; supplementary material Movie 6). Similar to SPH vesicles, APP vesicles that were associated with moving proteasomes were found to move in both an anterograde and retrograde direction (Fig. 6D,I). To test further whether other membranes, such as the endolysosome vesicles, correlate with proteasome movement, we transfected neurons with α4–YFP and stained lysosomes with a live-cell tracer (lysotracker-red, Fig. 6E; supplementary material Movie 7). Interestingly, we found a higher amount of α4–YFP moving with lysosomes in a retrograde direction compared with α4–YFP and lysosomes moving in an anterograde direction (Fig. 6F,I). Finally, proteasome movement was analyzed together with a mitochondria tracer (mitotracker-red, Fig. 6G; supplementary material Movie 8), which showed α4–YFP and mitochondria with common trajectories ('shared particles') in both an anterograde and retrograde direction (Fig. 6H,I). Controls that were performed prior to movie acquisition showed no bleed-through of the fluorescent labels in the red or green channel, confirming that cargos moving within the tested organelles contain proteasomes (supplementary material Fig. S4A). Quantification of all proteasome movement events observed in the sequential double-channel movies revealed that 49% of proteasomes were associated with lysosome vesicles, synaptophysin-containing vesicles, APP vesicles or mitochondria (Fig. 6J). Interestingly, 51% of the processive movement of proteasomes is unaccounted for by the membrane markers and organelles analyzed here, which suggests that other organelle compartments are also involved in proteasome transport (Fig. 6J). Potentially, a high association of α4–YFP with lysosomes could be interpreted as the protein being turned over by lysosomes. To exclude this possibility, we treated

Journal of Cell Science (2014) 127, 1537–1549 doi:10.1242/jcs.140780

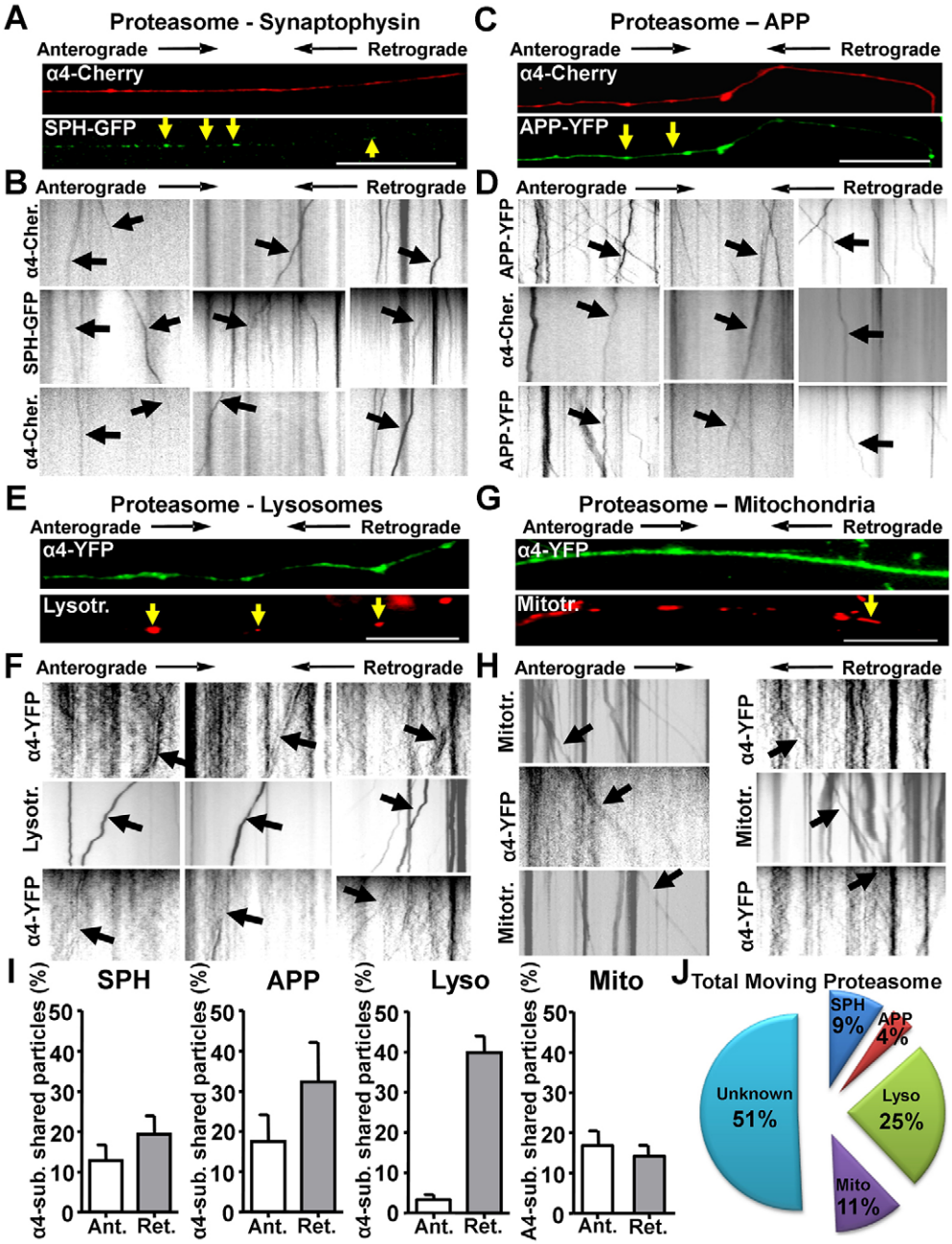

Fig. 6. Neuronal proteasomes associate with intracellular membrane organelles for movement. (A) Images from co-transfected neurons showing axons containing α4–Cherry (red) proteasome subunits and synaptophysin–GFP vesicles (arrows, SPH–GFP, green). Axons are oriented with cell bodies to the left and the synapse to the right. (B) Kymographs obtained from 45-second (8 Hz) double-color movies recorded in the red then green, then red channel (15 seconds each) corresponding to α4–Cherry (red) and SPH–GFP (green). Black arrows correspond to moving particles sharing the same trajectory (shared particles). (See supplementary material Movie 5.) (C,D) Images and kymographs from double-color movies recorded in similar conditions to A and B showing the shared processive movement of α4–Cherry and APP–YFP vesicles (arrows) (supplementary material Movie 6). (E,F) Images and kymographs from double-color movies recorded in the green then red, then green channel showing the shared movement of α4–YFP (green) and lysosome vesicles (arrows, lysotracker-red) (supplementary material Movie 7). (G,H) Images and kymograph from a double-color movie recorded in the green then red then green channel showing the shared movement of α4–YFP (green) and mitochondria (arrows, mitotracker-red). Scale bars: 20 μm. (See supplementary material Movie 8). (I) Quantification of shared green and red particles moving in an anterograde (Ant) or retrograde (Ret) direction for α4–Cherry with SPH–GFP (SPH), α4–Cherry with APP–YFP (APP), α4–YFP with lysotracker (Lyso) and α4–YFP with mitotracker (Mito). (J) The proportion of moving proteasomes that can be independently associated with synaptic vesicles (SPH), APP, lysosomes (Lyso) or mitochondria (Mito) from the total proteasome processive movement. Note the remaining 51% that moves associated with unknown cargos.

α4–YFP-transfected N2a cells with the lysosome inhibitor NH_4Cl (50 mM). As expected, full-length APP accumulated after treatment, but α4–YFP did not (supplementary material Fig. S4B), suggesting that α4–YFP is not being degraded by lysosomes under these test conditions. Taken together, these results suggest that actively transported proteasomes travel along the axon ‘hitch-hiking’ on multiple intracellular membranes for their delivery to distant neuronal locations.

DISCUSSION

Dysfunction of the UPS has been implicated in the abnormal accumulation of proteins that is observed in many neurodegenerative diseases (Bingol and Sheng, 2011; Rubinsztein, 2006). Axonal transport by the regulated action of molecular motors controls synaptic homeostasis through the delivery of cargo to distant locations (Goldstein, 2003) and by supporting the local protein clearance pathways. The experiments presented here constitute the first evidence that a fraction of neuronal proteasomes undergo fast microtubule- and motor-dependent transport with dynamics that correspond to membrane vesicle movement. Moreover, our results reveal three independent modes of proteasome motion by which proteasomes are widely distributed throughout neurons.

Cytoskeletal proteins are transported in axons by intracellular mechanisms, which implies slow component velocities of 1–10 mm/day (Lasek et al., 1984). The movement of these and many cytosolic proteins has been suggested to depend on the interaction with fast motors for their stochastic movement (Scott et al., 2011). Recently, the fast movement of a carrier, now identified as moving vesicles, has been suggested to drive the anterograde slow axonal transport of the synapsin proteins, suggesting that there are many modes for the movement for

soluble proteins (Tang et al., 2013). In this study, we tested whether the neuronal proteasome complex relies on different axonal transport mechanisms for movement in axons. Mouse sciatic nerve ligation experiments showed the accumulation of core and regulatory proteasome subunits at proximal ligation sites, indicating fast axonal transport of the 26S degradation complex *in vivo*. Moreover, protein polyubiquitination was increased after ligation, and enhancements in the proteasome degradation activity were mediated by the specific transport of the proteasome complex, and were not due to the ligation itself. These results highlight the relevance of a proteasome delivery system that, when impaired, can be implicated in the local ubiquitin-dependent protein accumulation observed after axonal injury or in pathological dystrophies (Hoopfer et al., 2006).

Previous experiments showing synaptic remodeling mediated by polyubiquitinated protein tagging and degradation imply a regulated mechanism of proteasome delivery in neurons (Bingol et al., 2010; Djakovic et al., 2009; Ehlers, 2003). Through fluorescent proteasome live-imaging experiments, we described the axonal motion properties of fluorescently tagged α4 core subunits in neurons of the central nervous system. Peripheral nerves showed a significant proximal accumulation of proteasomes with almost no distal accumulation, whereas central neurons displayed a similar proportion of α4 puncta moving in a processive manner in both anterograde and retrograde directions. This initial difference in proteasome dynamics might be explained by the distinct transport properties displayed between peripheral and central neurons, and the methods that suggest long-range accumulation *in vivo* during nerve ligation in mice compared with short high-resolution detection by live imaging in culture. The development of a high-resolution imaging setup and an accurate tracking system allowed the identification of at least three modes of proteasome motion in axons. We described a proportion of processive proteasome trajectories that display a superdiffusive motion where MSD dependence arises at values higher than 1.5 (Bruno et al., 2009; Brunstein et al., 2009; Robert et al., 2012). The range of velocities observed in this pattern of movement suggests that fast axonal transport of proteasomes is associated with organelles or vesicles that are transported by molecular motors. MSD analysis also revealed a highly represented diffusive behavior for the proteasome with a diffusion coefficient consistent with the proteasome molecular size in a medium that is more viscous than water, such as the axonema (Luby-Phelps, 2000; Popov and Poo, 1992). This important pattern of motion sustains the homogeneous distribution of proteasomes along the axon; however, it is insufficient to support the long-range transport of proteasomes to distant neuronal locations. Confined trajectories fitted well to a model where the constraint of particles is less than that exerted by elastic trapping (Jin et al., 2007), suggesting that this movement is limited in local cages of ~700 nm during the confined movement pattern. Further analyses are required to determine the origin of this trapping phenomenon and the linker that mediates the 'waiting time' that proteasomes spend in this non-transport mode.

In central neurons, fast activity-dependent recruitment of proteasomes to dendritic spines has been suggested to be a regulated process that is involved in protein degradation (Bingol and Schuman, 2006). Recent experiments using yeast two-hybrid assays and immunoprecipitations in cells have described an association of proteasomes with the motor machinery that is mediated by Ecm29 (Gorbea et al., 2010). To test the role of kinesin-1 in the long-range movement of proteasomes in axons, we knocked down expression of *kif5b* using a specific shRNA (Encalada et al., 2011). The high-accuracy tracking of processive trajectories allowed the determination of segmental velocities for actively transported proteasomes. Interestingly, this analysis yielded detailed information about the selective reduction in the density of anterograde segmental velocities exerted by kinesin-1 defects, which suggests that the overall transport flux was impaired, and not the properties of proteasome movement. This can be explained by a reduction of the number of active kinesins involved in transport upon treatment with shKif5b but that the biophysical properties of active kinesins are not affected. The mean retrograde velocity, which is driven by dynein, is enhanced in cells treated with shKif5b and can be explained by a recent report that showed that dyneins work collectively within cells and that their velocity is sensitive to opposing load (Rai et al., 2013). KIF5B knockdown showed that proteasome dynamics have a partial dependency on kinesin-1 and are consistent with the idea that the 26S proteasome is 'hitch-hiking' on different cargos in order to move. Interestingly, our results fit a model in which cytosolic proteins are transported by different types of movement – including the contribution of vesicle carriers under fast axonal transport (Scott et al., 2011; Tang et al., 2013). Furthermore, by high-resolution imaging and single-particle tracking, we identified and characterized diffusive modes of transport and actively driven transport that mediate the distribution of proteasomes within axons. We showed different types of fast moving vesicles and membrane organelles that drive the active transport of proteasomes. In addition, within our characterization, we identified the presence of confined proteasomes that could be interpreted as proteasomes that are trapped during a process that might involve the specific degradation of polyubiquitinated proteins.

Different lipid interaction experiments performed in yeast and *in vitro* suggest that proteasome complexes can associate with membranes (Kalies et al., 2005; Newman et al., 1996). Indeed, our current findings of similar fractionation profiles for different proteasome subunits in sucrose gradients suggest that assembled complexes are associated with membranes. In addition, synaptosome vesicle enrichment showed the presence of subunits from the 20S core and the 19S regulatory lid, suggesting that the ubiquitin-dependent 26S proteasome can associate with synaptic vesicles. To characterize further the membrane compartments in which proteasomes with processive trajectories can take over the transport processes, we recorded sequential movies in two fluorescent channels to find proteasome trajectories that were shared with different moving cargos. Despite the amount of diffusive proteasomes, interestingly, we found that some processive proteasome movement was shared with synaptic proteins, Golgi-derived APP-containing vesicles, endolysosomal vesicles and mitochondria. From our data, we conclude that lysosomes contribute primarily to the retrograde transport of the proteasome from synapses to cell bodies, whereas similar proportions of anterograde and retrograde movement were observed during the association of proteasomes with APP, synaptophysin or mitochondrial cargos. However, the cargo interactions that correspond with the remaining 50% of moving proteasomes still need to be identified to better explain the overall proteasome flux. In contrast with the slow axonal transport rates expected for large cytosolic protein complexes (Terada et al., 2010), here we describe the novel and surprising finding that the proteasome barrel is transported along axons by means of

'hitch-hiking' the fast and membrane-associated axonal transport mechanism. These results could also be interpreted as the transport of some membranous cargos along axons requiring co-transport with an assembled and functional proteasome complex. The association between proteasomes and moving cargos could be useful to degrade specific proteins during transport or upon arrival at the destination and, therefore, be distinct from cargos without proteasomes. The possibility that proteasome–membrane interactions mediate fast axonal transport of proteasomes in mobile vesicle units suggests that there is a direct link between proteasomes and membranes that requires further investigation. Modification of such a linker should change the mobility and/or distribution of the proteasome complex in polarized cells.

We have previously described that transport defects mediate the early neuronal pathways that lead to abnormal protein accumulation, protein deposition and enhanced axonopathies in different mouse models of neurodegeneration (Falzone et al., 2010; Falzone et al., 2009; Stokin et al., 2005). Similar transport defects can be further increased by proteasome inhibition (Tai et al., 2012; Tseng et al., 2008), which suggests that the neuronal protein degradation pathway closely interacts with the transport system. Taken together, our results reveal at least three different modes of transport for the proteasome and further provide evidence that assembled and functional proteasomes interact with membrane cargos and molecular motors for fast axonal transport. We propose a novel mechanism for the distribution and delivery of the 26S proteasome to distant neuronal locations that, when impaired, can lead to abnormal protein degradation phenotypes that are observed in many neurodegenerative diseases. We anticipate that these studies will facilitate our understanding of the defects in protein degradation that might arise because of impairments in proteasome mobilization.

MATERIALS AND METHODS

Mice

C57/BL6 mice were used to generate primary hippocampal cultures and sciatic nerve ligations. The mice were housed in temperature- and light-dark-controlled rooms under approved university protocols (UCSD-IACUC; UBA-456/2010).

Vectors

To generate α4 proteasome subunit cDNA, mRNA from mouse brain was obtained by RT-PCR using a first strand synthesis kit (Invitrogen). The α4 subunit cDNA was amplified by using PCR with the primers 5′-GCGCGATATCGCCACCATGAGCTACGACCGCGCCATCACC-3′ (including *Eco*RV and Kozak sites) and 5′-GCGCGCGGCCGCAGATG-CTTTCTTTTGCTTCTTCTTTTC-3′ (containing the *Not*I site). The α4 subunit sequence, without a stop codon, was subcloned in-frame with YFP into the pcDNA3-CMV-YFP plasmid to obtain the vector pcDNA3-CMV-α4-YFP. This vector was used to replace YFP with the mCherry fluorescent marker fused to the α4 subunit by using a subcloning strategy that utilized the *Not*I and *Apa*I restriction sites. pCDNA-CMV-EB3-RFP was kindly provided by Shuo-Chien Ling (UCSD, La Jolla, CA). pcDNA3-mCherry was provided by Nathan Shaner (UCSD, La Jolla, CA). pSPH-GFP was a kind gift from Louis Reichardt (UCSF, San Francisco, CA). Three shRNA–mCherry sequences against *kif5b*, from a kinesin lentiviral mini-library, in a pLL3.7 GW lentiviral vector with gateway entry modifications and an mCherry marker, were tested for reduction of levels of the KIF5B protein (Encalada et al., 2011).

Antibodies

Monoclonal antibodies against the following proteins were used: kinesin heavy chain (KHC-H2, Millipore), 20S proteasome subunit α5 (Biomol), tubulin (DM1α, Covance), ubiquitin (FK2, Biomol), ubiquitin (Chemicon). Polyclonal antibodies against the following proteins were used: proteasome α-β (pan-antibody recognizing subunits α5 or α7, and β1, β5 and β7, Biomol), β5, Mss1, PA28α (Biomol); YFP (Molecular Probes); APP, map2, tau, α-synuclein (Chemicon); KIF5B [provided by Gorazd B. Stokin (UCSD, La Jolla, CA)]; GDI, SPH, synaptotagmin (Synaptic System); dynein heavy chain, kinesin light chain 1 (Santa Cruz Biotechnology), syntaxin 13 (Bioss) and pJNK (Cell Signaling Technology). Secondary antibodies were: goat Alexa Fluor 568 and 488 anti-mouse or -rabbit IgG (Invitrogen). Horseradish-peroxidase-conjugated antibodies (Jackson Laboratories) were used in western blots.

Sciatic nerve ligation

Mouse sciatic nerves were ligated unilaterally at the hip, one or two nodes apart, by using surgical suture under isofluorane anesthesia. Mice were allowed to recover for 6 hours and then killed to obtain ligated and unligated nerves. For immunohistochemistry, nerves were embedded by using Tissue-Tek and then frozen by using a cryostat for sectioning later. For biochemical analyses, equal lengths of proximal, distal and unligated nerves were homogenized in sample buffer, and equal protein amounts were analyzed by using SDS-PAGE. All surgical procedures performed in adult C57/BL6 mice were approved by the University of California at San Diego Animal Committee (IACUC).

Immunofluorescent staining and quantification

Sciatic nerves were dissected and post-fixed 2 hours in 4% paraformaldehyde in PBS. Nerves were incubated overnight in 20% sucrose, embedded in Tissue-Tek Optimum Cutting Temperature (OCT) medium and frozen in dry-ice-cooled methanol. Serial 15-µm cryostat sections were cut and mounted onto coated slides (Fisher Scientific). Sections were permeabilized and blocked with 10% goat serum, 0.1% Triton X-100 in PBS for 30 minutes and incubated with the indicated primary antibodies overnight at 4℃. Samples were then incubated with Alexa-Fluor-conjugated secondary antibodies for 3 hours at room temperature. Low-resolution images were acquired by using a 20× lens (NA: 0.75) on a Nikon TE2000 microscope. Integrated fluorescence intensity measurements were extracted from images obtained under similar imaging conditions comparing equal areas of proximal, distal and unligated nerves, and normalized to the staining for phosphorylated neurofilaments. Normalized proteasome fluorescence intensity was plotted relative to the unligated condition. High-resolution cross-section images were observed by using a 60× or 100× lens (NA: 1.40) on an Olympus FV1000 confocal microscope.

Proteasome activity assay

Quantification of proteasome activity from extracts was measured by fluorogenic peptide hydrolysis (N-succinyl–Leu-Leu-Val-Tyr–7-amino-4-methylcoumarin, Biomol). Fluorescence measurements corresponding to proteasome activity (λ380–460) were calibrated using a range of 5 to 80 µg of total protein. Protein homogenate (40 µg) from proximal or unligated nerves was used to evaluate proteasome-dependent hydrolysis.

Immunoprecipitations

Controls or N2a cells transfected with pcDNA3-CMV-α4-YFP were homogenized in binding buffer (Tris-HCl 150 mM, NaCl 50 mM, NP40 0.1%, pH 7.5 and protease inhibitors) on ice and centrifuged for 10 minutes at 12,000 ***g*** at 4℃. Protein content was quantified by using 2 µl of supernatant in a bicinchoninic acid assay (BCA, Pierce). 500 µg of protein was pre-cleared with agarose beads and then incubated with the antibody against the α-β proteasome subunits overnight at 4℃. Protein-G–agarose beads that had been pre-washed overnight were incubated with the homogenate fraction plus primary antibody in binding buffer for 3 hours at 4℃. Beads were pelleted down and washed three times for 20 minutes with binding buffer and four times with PBS. Bound material was eluted by boiling beads in 1.5× sample buffer for 10 minutes and loaded in SDS-PAGE gel.

Journal of Cell Science (2014) 127, 1537–1549 doi:10.1242/jcs.140780

Primary hippocampal cultures and N2a cells

Culture of hippocampal cells was as described previously (Falzone and Stokin, 2012). Briefly, newborn hippocampal brain regions from C57/BL6 mice were dissected on postnatal day 1. Hippocampi were incubated in a 0.22-µm-filtered mixture of 45 U of papain in PBS enriched with 0.05% of DNase for 20 minutes at 37℃ and then triturated by gentle pipetting in 10% fetal bovine serum (FBS) in Dulbecco's modified Eagle's medium. Cells were grown in 500 µM L-glutamine and Neurobasal medium supplemented with B27 on poly-D-lysine-coated coverslips at 37℃ under 5% CO_2. Neurons transfected using Lipofectamine 2000 (Invitrogen) between days 7–10 for 16–20 hours were used for movie acquisition. Mouse neuroblastoma N2a cells (American Type Culture Collection) were propagated using 0.25% trypsin and grown at 37℃ under 5% CO_2 in Dulbecco's minimal essential media supplemented with 10% FBS, 1% penicillin and streptomycin, and 1% glutamax. N2a cells were transfected using polyethylenimine using a 2:1 ratio PEI:DNA following standard protocols.

Movie acquisition and kymograph analysis

Imaging and kymograph analysis was as described previously (Falzone and Stokin, 2012). Briefly, α4–YFP movement in neurons was recorded by using an inverted epifluorescent microscope (Olympus IX81) connected to a CCD camera (Olympus DP71/12.5 megapixels) and driven by a dynamic positioning. Cultures were kept under a 60× lens (NA: 1.40) at 37℃ using a heating stage and under 5% CO_2 by using a CO_2 chamber (Olympus). At 16–20 hours after transfection, cells were recorded. Directionality was determined by tracking axons at distance (2 fields) from cell bodies and imaging was performed away from cell bodies and projection tips. The pCMV-EB3-RFP vector was used to confirm plus-end-directed polymerization of the microtubules in axons (supplementary material Fig. S2). Continuous 30-second stacks (224 frames) at 125 mseconds/frame rate (8 Hz) were collected for α4–YFP. Sequential double-color movies were generated under green and red filters for 15 seconds each for α4–YFP with mitotracker (Invitrogen) and α4–YFP with lysotracker (Invitrogen), or α4–Cherry with APP–YFP and α4–Cherry with SPH–GFP. Shared particles were identified as those particles that moved in the green channel and continued in the red channel and then appeared back in the green channel with the same direction and speed. These particles were then quantified. Pixel size was adjusted to 0.13 µm. Kymographs were plotted with Image J using the multiple kymograph plug-in, and average net velocities, distance and directionality were extracted for analyses. High-resolution movies were recorded using a 100× lens (NA: 1.40) and a CMOS camera (Hamamatsu ORCA/Flash 2.8 megapixels) driven by HCImage controller (Hamamatsu Photonics, Japan). Continuous 10-second stacks (500 frames) at a rate of 20 mseconds/frame (50 Hz) were collected for α4–YFP. Pixel size was adjusted to 0.143 µm. Kymographs were plotted with ImageJ using the multiple kymograph plug-in and processed using MATLAB routines (The Mathworks, Natick, MA).

High spatio-temporal tracking and analysis of trajectories

A tracking algorithm was developed to recover trajectories of fluorescent proteasomes with a robust signal-to-noise ratio of >4 from kymographs with an error <20 nm. A rectangular region of interest (ROI) was selected, which could contain more than one particle. After that, the algorithm analyzes the first line of ROI within the kymograph, corresponding to the intensity profile along the axon, and searches for the maximum of intensity of the profile using a neural network smoothing procedure. The algorithm then goes to the next line of the ROI and searches the for the new maximum nearby. This procedure continues until the entire ROI is analyzed. The coordinates of the particle are recovered with subpixel resolution. In cases where the tracking was lost owing to crowding or enhanced background noise, the tracking was discarded. For each recovered trajectory, the mean square displacement (MSD) was calculated as follows:

$$\mathrm{MSD}\ (\tau) = \langle (x(t) - x(t+\tau))^2 \rangle, \quad (1)$$

where x is the coordinate of the proteasome along the axon, t and τ are the absolute and lag times, respectively, and the brackets represent the time average. This calculation was performed for $\tau < 10\%$ of the total time of the trajectory (Saxton and Jacobson, 1997). The MSD data were fitted with an anomalous diffusion model:

$$\mathrm{MSD} = A\tau^{\alpha} + B, \quad (2)$$

where A depends on the motion properties of the particle and B is the residual MSD (Brunstein et al., 2009; Nelson et al., 2009). The exponent α can take values between 0 and 2 (Brangwynne et al., 2009; Bruno et al., 2009). Trajectories were classified as actively driven ($\alpha > 1.5$), diffusive ($0.9 < \alpha < 1.1$) or confined ($\alpha < 0.5$) depending on the value of the exponent obtained from the fitting of Eqn 2 to the MSD data. Trajectories with α values that did not fulfill these criteria were discarded. Segmental velocities were determined from actively driven trajectories that were further divided into segments of 20 points. A linear regression of the position versus time plot was performed, and the segmental velocity was computed from the slope and included if the value $r^2 > 0.75$ (Levi et al., 2006). The diffusion coefficient (D) for the proteasome was obtained from diffusive trajectories with MSDs scaling to a lineal regression considering the slope equal to 2DC. Theoretical D in water was calculated by: $D = kT/6\pi hr$, considering the proteasome radius as 14.72 nm (Bohn et al., 2010). The size of the region of confinement (Rc) was determined as: $Rc = \sqrt{\langle MSD(\tau p)\rangle - MSD(0)}$ where $\langle MSD(\tau p)\rangle$ is the value of the MSD averaged for all times τ_p belonging to the plateau and MSD(0) is the value of the MSD for $\tau \rightarrow 0$.

Synaptosomes

Purification of synaptosomes has been described previously (Abe et al., 2009). Briefly, homogenized mouse brain cortices treated at 4℃ (0.3 M sucrose, 4 mM HEPES pH 7.5 and protease inhibitors) were centrifuged for 10 minutes, 800 ***g***, to obtain a P1 pellet and S1 supernatant. P2 and S2 were obtained by centrifuging S1 for 15 minutes at 9200 ***g***. A similar procedure was repeated to obtain P2′ which was then subjected to hypotonic shock with nine volumes of cold water. The solution was exchanged into 4 mM HEPES pH 7.5. Synaptic vesicle (LS1) and plasma membrane (LP1) fractions were obtained by centrifugation, 20 minutes at 25,000 ***g***. The synaptosome fraction (LP2) was obtained by sedimenting LS1 on a 38% sucrose cushion, 2 hours at 165,000 ***g***.

Sucrose density gradient

Briefly, cells harvested in cold PBS with protease inhibitor were centrifuged for 5 minutes at 2000 ***g*** at 4℃. The pellets were re-suspended with a Teflon glass potter in sucrose buffer (8% sucrose, 4 mM HEPES, EDTA 2 mM, EGTA 2 mM pH 7.5 and protease inhibitors) and centrifuged for 10 minutes at 12,000 ***g***. The supernatant was mixed with an equal volume of 62% sucrose buffer and was then bottom loaded, and 2.5 ml of 35%, 25% and 8% sucrose were sequentially added. Continuous gradients were generated by centrifugation for 16 hours at 100,000 ***g*** at 4℃. Fractions of 1 ml were methanol and chloroform precipitated and re-suspended in sample buffer.

Particle density distribution function analysis for confined trajectories

Particle density distribution function (PDDF) distinguished three different models of confinement: (1) a harmonic potential $U(r) = Uo\ r^2$, where particles are bound by a spring-like force-producing mechanism; (2) a cone potential $U(r) = Uo\ r$, where particles are trapped by a softer potential than that of the harmonic one; and (3) a r^4 potential $U(r) = Uo\ r^4$, which is harder than the spring potential where U(r) is the potential function, r the radius from the potential origin and Uo the potential strength. Thus, the normalized PDDF is given by: $PDDF(r)/PDDF(0) = e^{-U(r)/KBt}$ where KB is the Boltzmann constant and t is the absolute temperature. The PDDF was calculated for the position data as: $PDDF(x) = N(x)/Dx$ where Dx is the distribution

Journal of Cell Science

resolution and N(xo) is the number of events. Distribution was normalized by PDDF(0) for nonlinear least squares regression of Boltzmann distribution functions.

Statistical analysis

Values are expressed as means±standard error of the mean (s.e.m.) for the indicated number of independent experiments or corresponding particles (n). The normal distribution of the samples was assessed prior to analysis of significance. A two-tailed Student's t-test was used to compare differences between groups. A nonparametric Mann–Witney test was used when samples did not reach normality. Statistical analyses were performed using Graph-pad or MATLAB software.

Acknowledgements

We thank Fernanda Ledda (IBCN, Buenos Aires, Argentina), Gustavo Paratcha (IBCN, Buenos Aires, Argentina) and Gorazd Stokin for helpful discussion on data interpretation and presentation; Elizabeth Roberts and Andrea Pecile for their excellent technical assistance, Shuo-Chien Ling for providing the CMV-EB3-RFP plasmid (UCSD, La Jolla, CA). We thank Roux-Ocefa (Buenos Aires, Argentina) for kindly contributing basic reagents.

Competing interests

The authors declare no competing interests.

Author contributions

T.L.F., L.B. and L.S.G. conceived and designed the experiments; M.G.O., M.A., A.A., L.E.C., V.P.D. and T.L.F. performed the experiments. M.G.O., M.A. and T.L.F. analyzed the data. S.E. and V.P.D. contributed reagents, materials and analysis. The paper was written by T.L.F., L.B. and L.S.G.

Funding

This work was supported by grants from Alzheimer Association [grant number NIRG10-172840 to T.L.F]; and from Agencia Nacional de Promoción Científica y Tecnológica, Argentina [grant number PICT 2011-0293 to T.L.F.]. M.G.O. is the recipient of the Lanari's fellowship from Universidad de Buenos Aires. L.E.C. and V.P.D. are recipients of fellowships from The Consejo Nacional de Investigaciones Científicas y Técnicas (CONICET).

Supplementary material

Supplementary material available online at
http://jcs.biologists.org/lookup/suppl/doi:10.1242/jcs.140780/-/DC1

References

Abe, N., Almenar-Queralt, A., Lillo, C., Shen, Z., Lozach, J., Briggs, S. P., Williams, D. S., Goldstein, L. S. and Cavalli, V. (2009). Sunday driver interacts with two distinct classes of axonal organelles. *J. Biol. Chem.* **284**, 34628-34639.

Bence, N. F., Sampat, R. M. and Kopito, R. R. (2001). Impairment of the ubiquitin-proteasome system by protein aggregation. *Science* **292**, 1552-1555.

Bingol, B. and Schuman, E. M. (2006). Activity-dependent dynamics and sequestration of proteasomes in dendritic spines. *Nature* **441**, 1144-1148.

Bingol, B. and Sheng, M. (2011). Deconstruction for reconstruction: the role of proteolysis in neural plasticity and disease. *Neuron* **69**, 22-32.

Bingol, B., Wang, C. F., Arnott, D., Cheng, D., Peng, J. and Sheng, M. (2010). Autophosphorylated CaMKIIalpha acts as a scaffold to recruit proteasomes to dendritic spines. *Cell* **140**, 567-578.

Bohn, S., Beck, F., Sakata, E., Walzthoeni, T., Beck, M., Aebersold, R., Förster, F., Baumeister, W. and Nickell, S. (2010). Structure of the 26S proteasome from Schizosaccharomyces pombe at subnanometer resolution. *Proc. Natl. Acad. Sci. USA* **107**, 20992-20997.

Bossy-Wetzel, E., Schwarzenbacher, R. and Lipton, S. A. (2004). Molecular pathways to neurodegeneration. *Nat. Med.* **10 Suppl.**, S2-S9.

Brangwynne, C. P., Koenderink, G. H., MacKintosh, F. C. and Weitz, D. A. (2009). Intracellular transport by active diffusion. *Trends Cell Biol.* **19**, 423-427.

Bruno, L., Levi, V., Brunstein, M. and Despósito, M. A. (2009). Transition to superdiffusive behavior in intracellular actin-based transport mediated by molecular motors. *Phys. Rev. E Stat. Nonlin. Soft Matter Phys.* **80**, 011912.

Brunstein, M., Bruno, L., Desposito, M. and Levi, V. (2009). Anomalous dynamics of melanosomes driven by myosin-V in Xenopus laevis melanophores. *Biophys. J.* **97**, 1548-1557.

Ciechanover, A. and Brundin, P. (2003). The ubiquitin proteasome system in neurodegenerative diseases: sometimes the chicken, sometimes the egg. *Neuron* **40**, 427-446.

Djakovic, S. N., Schwarz, L. A., Barylko, B., DeMartino, G. N. and Patrick, G. N. (2009). Regulation of the proteasome by neuronal activity and calcium/calmodulin-dependent protein kinase II. *J. Biol. Chem.* **284**, 26655-26665.

Ehlers, M. D. (2003). Activity level controls postsynaptic composition and signaling via the ubiquitin-proteasome system. *Nat. Neurosci.* **6**, 231-242.

Encalada, S. E., Szpankowski, L., Xia, C. H. and Goldstein, L. S. (2011). Stable kinesin and dynein assemblies drive the axonal transport of mammalian prion protein vesicles. *Cell* **144**, 551-565.

Falzone, T. L. and Stokin, G. B. (2012). Imaging amyloid precursor protein in vivo: an axonal transport assay. *Methods Mol. Biol.* **846**, 295-303.

Falzone, T. L., Stokin, G. B., Lillo, C., Rodrigues, E. M., Westerman, E. L., Williams, D. S. and Goldstein, L. S. (2009). Axonal stress kinase activation and tau misbehavior induced by kinesin-1 transport defects. *J. Neurosci.* **29**, 5758-5767.

Falzone, T. L., Gunawardena, S., McCleary, D., Reis, G. F. and Goldstein, L. S. (2010). Kinesin-1 transport reductions enhance human tau hyperphosphorylation, aggregation and neurodegeneration in animal models of tauopathies. *Hum. Mol. Genet.* **19**, 4399-4408.

Goldstein, L. S. (2003). Do disorders of movement cause movement disorders and dementia? *Neuron* **40**, 415-425.

Gorbea, C., Pratt, G., Ustrell, V., Bell, R., Sahasrabudhe, S., Hughes, R. E. and Rechsteiner, M. (2010). A protein interaction network for Ecm29 links the 26 S proteasome to molecular motors and endosomal components. *J. Biol. Chem.* **285**, 31616-31633.

Hirokawa, N., Niwa, S. and Tanaka, Y. (2010). Molecular motors in neurons: transport mechanisms and roles in brain function, development, and disease. *Neuron* **68**, 610-638.

Hoopfer, E. D., McLaughlin, T., Watts, R. J., Schuldiner, O., O'Leary, D. D. and Luo, L. (2006). Wlds protection distinguishes axon degeneration following injury from naturally occurring developmental pruning. *Neuron* **50**, 883-895.

Jin, S., Haggie, P. M. and Verkman, A. S. (2007). Single-particle tracking of membrane protein diffusion in a potential: simulation, detection, and application to confined diffusion of CFTR Cl- channels. *Biophys. J.* **93**, 1079-1088.

Kalies, K. U., Allan, S., Sergeyenko, T., Kröger, H. and Römisch, K. (2005). The protein translocation channel binds proteasomes to the endoplasmic reticulum membrane. *EMBO J.* **24**, 2284-2293.

Karki, S. and Holzbaur, E. L. (1999). Cytoplasmic dynein and dynactin in cell division and intracellular transport. *Curr. Opin. Cell Biol.* **11**, 45-53.

Keck, S., Nitsch, R., Grune, T. and Ullrich, O. (2003). Proteasome inhibition by paired helical filament-tau in brains of patients with Alzheimer's disease. *J. Neurochem.* **85**, 115-122.

Keller, J. N., Hanni, K. B. and Markesbery, W. R. (2000). Impaired proteasome function in Alzheimer's disease. *J. Neurochem.* **75**, 436-439.

Lasek, R. J., Garner, J. A. and Brady, S. T. (1984). Axonal transport of the cytoplasmic matrix. *J. Cell Biol.* **99**, 212s-221s.

Levi, V., Serpinskaya, A. S., Gratton, E. and Gelfand, V. (2006). Organelle transport along microtubules in Xenopus melanophores: evidence for cooperation between multiple motors. *Biophys. J.* **90**, 318-327.

Luby-Phelps, K. (2000). Cytoarchitecture and physical properties of cytoplasm: volume, viscosity, diffusion, intracellular surface area. *Int. Rev. Cytol.* **192**, 189-221.

Mengual, E., Arizti, P., Rodrigo, J., Giménez-Amaya, J. M. and Castaño, J. G. (1996). Immunohistochemical distribution and electron microscopic subcellular localization of the proteasome in the rat CNS. *J. Neurosci.* **16**, 6331-6341.

Murata, S., Yashiroda, H. and Tanaka, K. (2009). Molecular mechanisms of proteasome assembly. *Nat. Rev. Mol. Cell Biol.* **10**, 104-115.

Nelson, S. R., Ali, M. Y., Trybus, K. M. and Warshaw, D. M. (2009). Random walk of processive, quantum dot-labeled myosin Va molecules within the actin cortex of COS-7 cells. *Biophys. J.* **97**, 509-518.

Newman, R. H., Whitehead, P., Lally, J., Coffer, A. and Freemont, P. (1996). 20S human proteasomes bind with a specific orientation to lipid monolayers in vitro. *Biochim. Biophys. Acta* **1281**, 111-116.

Oddo, S. (2008). The ubiquitin-proteasome system in Alzheimer's disease. *J. Cell. Mol. Med.* **12**, 363-373.

Patrick, G. N. (2006). Synapse formation and plasticity: recent insights from the perspective of the ubiquitin proteasome system. *Curr. Opin. Neurobiol.* **16**, 90-94.

Popov, S. and Poo, M. M. (1992). Diffusional transport of macromolecules in developing nerve processes. *J. Neurosci.* **12**, 77-85.

Rai, A. K., Rai, A., Ramaiya, A. J., Jha, R. and Mallik, R. (2013). Molecular adaptations allow dynein to generate large collective forces inside cells. *Cell* **152**, 172-182.

Reis, G. F., Yang, G., Szpankowski, L., Weaver, C., Shah, S. B., Robinson, J. T., Hays, T. S., Danuser, G. and Goldstein, L. S. (2012). Molecular motor function in axonal transport in vivo probed by genetic and computational analysis in Drosophila. *Mol. Biol. Cell* **23**, 1700-1714.

Reits, E. A., Benham, A. M., Plougastel, B., Neefjes, J. and Trowsdale, J. (1997). Dynamics of proteasome distribution in living cells. *EMBO J.* **16**, 6087-6094.

Robert, D., Aubertin, K., Bacri, J. C. and Wilhelm, C. (2012). Magnetic nanomanipulations inside living cells compared with passive tracking of nanoprobes to get consensus for intracellular mechanics. *Phys. Rev. E Stat. Nonlin. Soft Matter Phys.* **85**, 011905.

Rubinsztein, D. C. (2006). The roles of intracellular protein-degradation pathways in neurodegeneration. *Nature* **443**, 780-786.

Saxton, M. J. and Jacobson, K. (1997). Single-particle tracking: applications to membrane dynamics. *Annu. Rev. Biophys. Biomol. Struct.* **26**, 373-399.

Scott, D. A., Das, U., Tang, Y. and Roy, S. (2011). Mechanistic logic underlying the axonal transport of cytosolic proteins. *Neuron* **70**, 441-454.

Stokin, G. B. and Goldstein, L. S. (2006). Axonal transport and Alzheimer's disease. *Annu. Rev. Biochem.* **75**, 607-627.

Stokin, G. B., Lillo, C., Falzone, T. L., Brusch, R. G., Rockenstein, E., Mount, S. L., Raman, R., Davies, P., Masliah, E., Williams, D. S. et al. (2005). Axonopathy and transport deficits early in the pathogenesis of Alzheimer's disease. *Science* **307**, 1282-1288.

Tai, H. C. and Schuman, E. M. (2008). Ubiquitin, the proteasome and protein degradation in neuronal function and dysfunction. *Nat. Rev. Neurosci.* **9**, 826-838.

Tai, H. C., Serrano-Pozo, A., Hashimoto, T., Frosch, M. P., Spires-Jones, T. L. and Hyman, B. T. (2012). The synaptic accumulation of hyperphosphorylated tau oligomers in Alzheimer disease is associated with dysfunction of the ubiquitin-proteasome system. *Am. J. Pathol.* **181**, 1426-1435.

Tang, Y., Scott, D., Das, U., Gitler, D., Ganguly, A. and Roy, S. (2013). Fast vesicle transport is required for the slow axonal transport of synapsin. *J. Neurosci.* **33**, 15362-15375.

Terada, S., Kinjo, M., Aihara, M., Takei, Y. and Hirokawa, N. (2010). Kinesin-1/Hsc70-dependent mechanism of slow axonal transport and its relation to fast axonal transport. *EMBO J.* **29**, 843-854.

Tseng, B. P., Green, K. N., Chan, J. L., Blurton-Jones, M. and LaFerla, F. M. (2008). Abeta inhibits the proteasome and enhances amyloid and tau accumulation. *Neurobiol. Aging* **29**, 1607-1618.

Upadhya, S. C., Ding, L., Smith, T. K. and Hegde, A. N. (2006). Differential regulation of proteasome activity in the nucleus and the synaptic terminals. *Neurochem. Int.* **48**, 296-305.

Yi, J. J. and Ehlers, M. D. (2007). Emerging roles for ubiquitin and protein degradation in neuronal function. *Pharmacol. Rev.* **59**, 14-39.

Zhao, Y., Hegde, A. N. and Martin, K. C. (2003). The ubiquitin proteasome system functions as an inhibitory constraint on synaptic strengthening. *Curr. Biol.* **13**, 887-898.